PERGAMON

Chemosphere 53 (2003) 437–446

CHEMOSPHERE

www.elsevier.com/locate/chemosphere

# Reduction of $Ag^{I}$, $Au^{III}$, $Cu^{II}$, and $Hg^{II}$ by $Fe^{II}/Fe^{III}$ hydroxysulfate green rust ☆

Edward J. O'Loughlin [a,*], Shelly D. Kelly [a], Kenneth M. Kemner [a], Roseann Csencsits [b], Russell E. Cook [b]

[a] *Environmental Research Division, Argonne National Laboratory, Room E-137, Building 203, 9700 South Cass Ave., Argonne, IL 60439-4843, USA*

[b] *Materials Science Division, Argonne National Laboratory, Argonne, IL 60439-4843, USA*

Received 3 February 2003; received in revised form 9 May 2003; accepted 19 May 2003

**Abstract**

Green rusts are mixed $Fe^{II}/Fe^{III}$ hydroxides that are found in many suboxic environments where they are believed to play a central role in the biogeochemical cycling of iron. X-ray absorption fine structure analysis of hydroxysulfate green rust suspensions spiked with aqueous solutions of $AgCH_3COO$, $AuCl_n(OH)_{4-n}$, $CuCl_2$, or $HgCl_2$ showed that $Ag^{I}$, $Au^{III}$, $Cu^{II}$, and $Hg^{II}$ were readily reduced to $Ag^0$, $Au^0$, $Cu^0$, and $Hg^0$. Imaging of the resulting solids from the $Ag^{I}$-, $Au^{III}$-, and $Cu^{II}$-amended green rust suspensions by transmission electron microscopy indicated the formation of submicron-sized particles of $Ag^0$, $Au^0$, and $Cu^0$. The facile reduction of $Ag^{I}$, $Au^{III}$, $Cu^{II}$, and $Hg^{II}$ to $Ag^0$, $Au^0$, $Cu^0$, and $Hg^0$, respectively, by green rust suggests that the presence of green rusts in suboxic soils and sediments can have a significant impact on the biogeochemistry of silver, gold, copper, and mercury, particularly with respect to their mobility.



*Keywords:* Zero-valent; Silver; Gold; Copper; Mercury; XAFS

## 1. Introduction

The environmental chemistry of transition metals is highly dependent on their chemical speciation, which in turn profoundly impacts their physical, chemical, and biological activities. The speciation of transition metals in aquatic and terrestrial environments is a function of many parameters, including concentration, temperature, ionic strength, and the presence and concentrations of other chemical components (pH in particular). In addition, many of the transition metals (e.g., V, Cr, Mn, Fe, Co, Cu, Tc, Ag, and Hg) have multiple valence states within the range of redox conditions encountered in surface or near-surface environments. The chemical properties of an element are often quite variable from one oxidation state to another, thus changes in valence state are typically accompanied by significant changes in bioavailability, toxicity, and mobility.

Ferrous iron ($Fe^{II}$) is one of the most abundant reductants typically present in aquatic and terrestrial environments under suboxic and anoxic conditions

☆ The submitted manuscript has been created by the University of Chicago as operator of Argonne National Laboratory under Contract No. W-31-109-ENG-38 with the US Department of Energy. The US government retains for itself, and others acting on its behalf, a paid-up, nonexclusive, irrevocable worldwide license in said article to reproduce, prepare derivative works, distribute copies to the public, and perform publicly and display publicly, by or on behalf of the government.

* Corresponding author. Tel.: +1-630-252-9902; fax: +1-630-252-2959.

*E-mail address:* oloughlin@anl.gov (E.J. O'Loughlin).

0045-6535/$ - see front matter © 2003 Elsevier Ltd. All rights reserved.
doi:10.1016/S0045-6535(03)00545-9

(Hering and Stumm, 1990; Lyngkilde and Christensen, 1992; Rügge et al., 1998). In these environments $Fe^{II}$ may be present as soluble organic and inorganic complexes, as surface complexes, and as a host of $Fe^{II}$-bearing mineral phases, including $Fe^{II}$-containing clays (e.g., smectites, vermiculites, and micas), ilmenite, magnetite, siderite, vivianite, ferrous sulfide, pyrite, and green rust. Although numerous studies have examined the reduction of transition metals by $Fe^{II}$-bearing clays, ferrous sulfide, pyrite, and magnetite (Bancroft and Hyland, 1990; Ilton et al., 1992; Peterson et al., 1996; White and Peterson, 1996; Scaini et al., 1997; Taylor et al., 2000; and many others), the reduction of transition metals by green rust has only recently been examined (Loyaux-Lawniczak et al., 1999, 2000; Williams and Scherer, 2001).

Green rusts are mixed $Fe^{II}/Fe^{III}$ hydroxides that have layered structures consisting of alternating positively charged hydroxide layers and hydrated anion layers. Green rusts typically form under near-neutral to alkaline conditions in suboxic environments and are often metastable intermediates in the transformation of $Fe^{II}$ to magnetite and $Fe^{III}$ oxyhydroxides (e.g., lepidocrocite and goethite). Green rusts are believed to play a central role in the redox cycling of Fe in aquatic and terrestrial environments. Although the characteristic bluish-green color of hydromorphic soils has long been presumed to be due to the presence of mixed $Fe^{II}/Fe^{III}$ hydroxide species (Ponnamperuma et al., 1967), the unambiguous identification of green rusts in suboxic soils and sediments has been complicated by the rapid oxidation of these compounds upon exposure to air. However, in spite of this difficulty, direct evidence for the presence of green rusts in hydromorphic soils has recently been reported (Trolard et al., 1997; Abdelmoula et al., 1998). Moreover, Bourrié et al. (1999) has suggested that the solubility of Fe in the soil solutions of hydromorphic soils is controlled by equilibrium with green rusts. Green rusts are observed as products of the metabolic activity of bacteria known to be key players in the biogeochemical redox cycling of Fe in aquatic and terrestrial environments. Various strains of the dissimilatory iron-reducing bacterium *Shewanella putrefaciens* produce green rusts as products of the bioreduction of hydrous ferric oxide and lepidocrocite (Fredrickson et al., 1998; Kukkadapu et al., 2001; Parmar et al., 2001; Glasauer et al., 2002; Ona-Nguema et al., 2002), and green rusts are also observed as products of the anaerobic biooxidation of $Fe^{II}$ by *Dechlorosoma suillum* (Chaudhuri et al., 2001).

Recent research has shown that green rusts are capable of reducing a number of organic and inorganic contaminants, suggesting that green rusts may be highly reactive reductants in suboxic environments. Several studies have shown that green rusts reduce nitrate and nitrite to ammonia (Hansen et al., 1994, 2001). Green rusts have also been shown to reduce selenate ($Se^{VI}$) to $Se^0$ and $Se^{-II}$ (Myneni et al., 1997; Refait et al., 2000), chromate ($Cr^{VI}$) to $Cr^{III}$ (Loyauz-Lawniczak et al., 2000; Williams and Scherer, 2001), and $U^{VI}$ to $U^{IV}$ (O'Loughlin et al., 2003). The reductive dehalogenation of several halogenated hydrocarbons, including carbon tetrachloride, hexachloroethane, and 1,2-dibromoethane (EDB) has also been reported (Erbs et al., 1999; O'Loughlin and Burris, in press). Moreover, the addition of $Ag^{I}$, $Au^{III}$, or $Cu^{II}$ to aqueous green rust suspensions was recently shown to catalyze the reductive dehalogenation of carbon tetrachloride (O'Loughlin et al., 2003).

In this study we use X-ray absorption spectroscopy and transmission electron microscopy to examine the reduction of $Ag^{I}$, $Au^{III}$, $Cu^{II}$, and $Hg^{II}$ by hydroxysulfate green rust.

## 2. Experimental section

### 2.1. Chemicals

Iron(II) sulfate heptahydrate (99+%), copper(II) chloride (99.999%), silver(I) acetate (99.999%), and mercury(II) chloride (99.999%) were obtained from Aldrich (Milwaukee, WI). Gold(III) chloride was purchased from Sigma (St. Louis, MO). Concentrated nitric acid (trace metal grade) was obtained from Fisher (Pittsburgh, PA).

Hydroxysulfate green rust ($GR_{SO_4}$), a green rust in which the interlayer anion is $SO_4^{2-}$, was synthesized by air oxidation of a 1.0 M ferrous sulfate solution. Briefly, 278 g of $FeSO_4 \cdot 7H_2O$ were dissolved in 1 l of high-purity (18 MΩ-cm) water on a magnetic stirrer under ambient atmosphere. Upon dissolution, 1.0 M NaOH was added dropwise until the pH remained stable at 7.0, at which point the $GR_{SO_4}$ suspension was placed in an anoxic glove box (4–6% $H_2$ in $N_2$). The green rust was recovered by centrifugation and subsequently washed four times with high-purity water. Analysis of the purified material by X-ray diffraction (XRD) indicated that $GR_{SO_4}$ was the only observed product.

### 2.2. Experimental setup

The reaction system consisted of 250-ml polypropylene centrifuge bottles with O-ring sealed caps. Unless otherwise indicated, sample preparation and handling were conducted in a glove box with an atmosphere of 4–6% $H_2$ in $N_2$. Reactions were initiated by adding 25 ml of 500 μM–2.0 mM $Ag^{I}$, $Au^{III}$, $Cu^{II}$ or $Hg^{II}$ to 0.5 g of $GR_{SO_4}$ in 100 ml of high-purity water with constant mixing. After 30 min, a 10-μl subsample of the suspensions to which $Ag^{I}$, $Au^{III}$, or $Cu^{II}$ was added was removed and deposited on gold (for samples containing Ag or Cu) or copper (for samples containing Au) transmis-

sion electron microscopy (TEM) grids with holey carbon films; because of the volatility of $Hg^0$, $Hg^{II}$-amended green rust samples were not prepared for TEM. The samples were air-dried under anoxic conditions for at least 12 h prior to TEM imaging. The remainder of each of the $Ag^{I}$-, $Au^{III}$-, $Cu^{II}$-, or $Hg^{II}$-amended green rust suspensions (hereafter designated as AgGR, AuGR, CuGR, and HgGR, respectively) was centrifuged. The supernatants were saved for Ag, Au, Cu, and Hg analysis by inductively coupled plasma-optical emission spectroscopy (ICP-OES). The pellets were resuspended in deoxygenated, high-purity water and centrifuged again; the green rust pellets were washed two more times in this manner. After the final washing, subsamples of the wet pastes were removed for analysis by X-ray absorption fine structure (XAFS) spectroscopy and XRD.

### 2.3. ICP-OES analysis

A PerkinElmer Optima 4300DV ICP-OES was used to measure the concentration of Ag, Au, Cu, and Hg in the supernatants of the centrifuged AgGR, AuGR, CuGR, and HgGR suspensions by using the ICP conditions listed in Table 1. Samples for ICP-OES analysis were spiked with concentrated nitric acid to achieve a concentration of 5% nitric acid by volume.

### 2.4. TEM imaging

The samples for TEM imaging were stored under anoxic conditions, except for a brief (1–2 s) exposure to air during transfer of the sample holder to the vacuum chamber on the microscope. Specimens were imaged by using the bright-field imaging mode of an FEI Tecnai F20 scanning transmission electron microscope (STEM) operating in TEM mode at 200 kV and in a JOEL 4000EXII high resolution transmission electron microscope (HRTEM) at 400 kV in the Electron Microscopy Collaborative Research Center at Argonne National Laboratory. Energy-dispersive X-ray (EDX) spectra were collected with an EDAX detector using an electron beam diameter of approximately 1 nm.

Table 1
ICP-OES operating conditions used for the determination of solution-phase Ag, Au, Cu, and Hg concentrations

| Parameter | Setting |
|---|---|
| View mode | Radial |
| View height | 15 mm |
| Plasma | Argon |
| RF generator power | 1400 W |
| Shear gas | Air |
| Gas flow: plasma | 17 ml $min^{-1}$ |
| Gas flow: auxiliary | 0.2 ml $min^{-1}$ |
| Gas flow: nebulizer | 0.6 ml $min^{-1}$ |
| Sample aspiration rate | 1.5 ml $min^{-1}$ |
| Detector | CCD |
| Emission line: Ag | 328.068 nm |
| Emission line: Au | 267.601 nm |
| Emission line: Cu | 327.393 nm |
| Emission line: Hg | 253.652 nm |
| Rinse delay | 30 s |
| Read delay | 60 s |
| Source equilibration time | 30 s |
| Read | Peak area |
| Number of replicates | 3 |

### 2.5. XRD analysis

The XRD analysis of $GR_{SO_4}$, AgGR, AuGR, CuGR, and HgGR was performed using a Rigaku MiniFlex X-ray diffractometer with Ni-filtered Cu K$\alpha$ radiation. Samples for XRD analysis were prepared by mixing the wet pastes with glycerol to minimize oxidation (Hansen and Koch, 1998) and prepared as smears on 22-mm-wide glass plates. The samples were scanned between 6° and 80° 2$\theta$ at a speed of 1° 2$\theta$ $min^{-1}$. The XRD data were processed with Jade 6.0 (Materials Data, Inc., Livermore, CA).

### 2.6. XAFS analysis

Fluorescence XAFS measurements were made on wet, homogeneous AgGR, AuGR, and CuGR pastes as well as on aqueous solutions of 10 mM $Au^{III}Cl_n(OH)_{4-n}$ and 10 mM $CuCl_2$. Transmission XAFS measurements were made on wet, homogeneous HgGR pastes; on standard $Ag^0$, $Au^0$, and $Cu^0$ foils; and on $Ag_2O$(s) and HgO(s) standards (both prepared as fine powder films on Kapton tape). The wet pastes and aqueous samples were mounted in holes machined in Plexiglas slides, and the holes were covered with Kapton film held in place with Kapton tape. Aqueous solutions of reduced resorufin (a redox indicator dye; solutions of reduced resorufin will turn from colorless to pink upon exposure to molecular oxygen) mounted in this manner and exposed to air remained colorless for more than 8 h, indicating that such sample mounts are effective for excluding oxygen from samples during analysis. XAFS data for liquid $Hg^0$ at 299 K were generously provided by Dr. Adriano Filipponi (Ottaviano et al., 1994).

The XAFS data were collected at the Materials Research Collaborative Access Team (MR-CAT) sector 10-ID beamline (Segre et al., 2000) at the advanced photon source (APS) at Argonne National Laboratory. Data were collected for both X-ray absorption near edge structure (XANES), an in situ probe that provides information about the oxidation state and coordination geometry of the absorbing atom (Durham, 1988), and extended X-ray absorption fine structure (EXAFS), which provides information on the type and number of the atoms surrounding the absorbing atom, as well as

the radial distances to those atoms (Stern, 1988). Data for XANES and EXAFS spectra were collected at the Ag and Cu K-edges and the Au and Hg $L_{III}$-edges.

The energy of the incident X-rays was selected by a Si (1 1 1) double-crystal monochromator. X-rays with higher harmonic energies were rejected by using a Rh (for Au, Cu, and Hg measurements) or Pd (for Ag measurements) mirror. The undulator was scanned or tapered to reduce the variation of the incident X-ray intensity to less than 30% over the EXAFS region (~1000 eV). The incident and transmitted X-ray intensities were monitored with ion chambers. Filtered fluorescent X-ray intensity was monitored with an ion chamber detector in the Stern–Heald geometry (Stern and Heald, 1979). Monochromator energy was monitored by using reference materials as described by Cross and Frenkel (Cross and Frenkel, 1998). The codes contained in the IFEFFIT package (Newville, 2001) were used to analyze the data. For each sample, several data sets were collected, step-height-normalized, and then averaged to produce the final spectra. The $\chi(k) * k^2$ data were produced by removing the step-like background function from the normalized spectra according to standard procedures (Newville et al., 1993). Parameters specific to each sample are in Table 2.

## 3. Results

Added as aqueous solutions of $CH_3CO_2Ag$, $HAuCl_4$, $CuCl_2$, and $HgCl_2$, respectively, $Ag^I$, $Au^{III}$, $Cu^{II}$, and $Hg^{II}$ were rapidly removed from solution in green rust suspensions. Within 30 min after the addition of 50 μmol of $Ag^I$, $Au^{III}$, $Cu^{II}$, or $Hg^{II}$, solution-phase concentrations of Ag, Au, Cu, and Hg were reduced from 400 μM to 890 nM, 360 nM, 1.2 μM, and 1.7 μM, respectively; reductions in solution-phase concentrations of comparable magnitude were also observed in systems with lower initial loadings of $Ag^I$, $Au^{III}$, $Cu^{II}$, or $Hg^{II}$. These results indicate that nearly all of the silver, copper, gold, and mercury added to these systems rapidly became associated with the solid phase(s).

As previously discussed, XANES spectroscopy provides information on the oxidation state of an atom, as indicated by the energy of the adsorption edge; typically, the edge energy increases with increasing oxidation state. A comparison of the XANES spectra of AgGR, AuGR, CuGR, and HgGR with the relevant standards ($Ag^0$ foil and $Ag_2O$ for AgGR; $Au^0$ foil and 10 mM $HAuCl_4$ for AuGR; $Cu^0$ foil and 10 mM $CuCl_2$ for CuGR; and $Hg^0(l)$ and HgO for HgGR) clearly shows that $Ag^I$, $Au^{III}$, $Cu^{II}$, and $Hg^{II}$ were reduced to $Ag^0$, $Au^0$, $Cu^0$, and $Hg^0$ (Fig. 1). XRD analysis of the AgGR, AuGR, CuGR, and HgGR pastes indicated that the reduction of $Ag^I$, $Au^{III}$, $Cu^{II}$, and $Hg^{II}$ to $Ag^0$, $Au^0$, $Cu^0$, and $Hg^0$ is accompanied by the partial oxidation of green rust to magnetite (Fig. 2).

Information on the local environment of Ag, Au, Cu, and Hg atoms in the AgGR, AuGR, CuGR, and HgGR samples is provided by the EXAFS data. The Ag K-edge, Au $L_{III}$-edge, Cu K-edge, and Hg $L_{III}$-edge background-subtracted, $k^2$-weighted $\chi(k)$ data from AgGR,

Table 2
Parameters for XAFS data collection for individual samples

| Sample | Edge | Mode | Gas in $I_0$[a] | Gas in $I_t$[b] | Gas in $I_f$[c] | Filter in $I_f$ | Monochromator reference |
|---|---|---|---|---|---|---|---|
| $Ag^0$ (foil) | Ag-K | Trans[d] | $N_2$ | Ar | | | $Ag^0$ foil |
| $Ag^I$ (finely powdered $Ag_2O$) | Ag-K | Trans | $N_2$ | Ar | | | $Ag^0$ foil |
| AgGR ($Ag^I$ added to GR suspension) | Ag-K | Fluo[e] | $N_2$ | | Kr | | $Ag^0$ foil |
| $Au^0$ (foil) | Au-$L_{III}$ | Trans | He:$N_2$ (1:1) | Ar:$N_2$ (1:1) | | | $Au^0$ foil |
| $Au^{III}$ (10 mM $AuCl_nOH_{4-n}$) | Au-$L_{III}$ | Fluo | He:$N_2$ (1:1) | | Ar | Ge (3)[f] | $Au^0$ foil |
| AuGR ($Au^{III}$ added to GR suspension) | Au-$L_{III}$ | Fluo | He:$N_2$ (1:1) | | Ar | Ge (3)[f] | $Au^0$ foil |
| $Cu^0$ (foil) | Cu-K | Trans | $N_2$ | $N_2$ | | | $Cu^0$ foil |
| $Cu^I$ (10 mM $CuCl_2$) | Cu-K | Fluo | $N_2$ | | Ar | Cr (3)[f] & Ni (6)[f] | $Cu^0$ foil |
| CuGR ($Cu^{II}$ added to GR suspension) | Cu-K | Fluo | $N_2$ | | Ar | Cr (3)[f] & Ni (6)[f] | $Cu^0$ foil |
| $Hg^{II}$ (finely powdered HgO) | Hg-$L_{III}$ | Trans | $N_2$ | $N_2$ | | | Se (3)[f] |
| HgGR ($Hg^{II}$ added to GR suspension) | Hg-$L_{III}$ | Trans | $N_2$:$H_2$ (2:1) | $N_2$:$H_2$ (2:1) | | | HgO |

[a] Incident X-ray intensity detector (ion chamber).
[b] Transmitted X-ray intensity detector (ion chamber).
[c] Fluorescence X-ray intensity detector (ion chamber in Stern–Heald geometry).
[d] Transmission.
[e] Fluorescence.
[f] Filter thickness (number of absorption lengths).

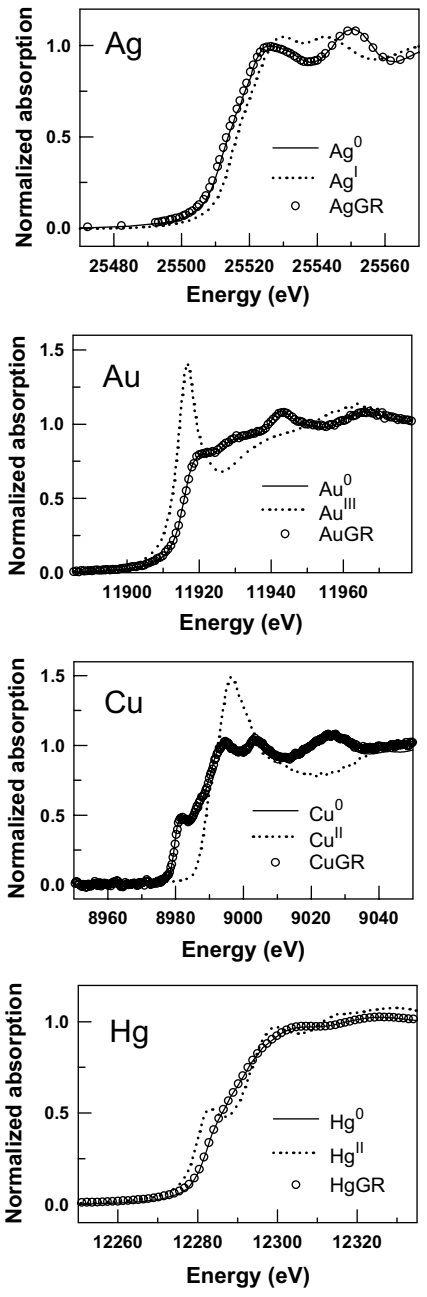


Fig. 1. Comparison of step-height-normalized Ag K-edge XANES spectra for $Ag^0$ (foil), $Ag^I$ ($Ag_2O$), and silver (added as $Ag^I$) in a green rust suspension (top); step-height-normalized Au $L_{III}$-edge XANES spectra for $Au^0$ (foil), $Au^{III}$ (10 mM $AuCl_n(OH)_{4-n}$), and gold (added as $Au^{III}$) in a green rust suspension (second from top); step-height-normalized Cu K-edge XANES spectra for $Cu^0$ (foil), $Cu^{II}$ (10 mM $CuCl_2$), and copper (added as $Cu^{II}$) in a green rust suspension (second from bottom); and step-height-normalized Hg $L_{III}$-edge XANES spectra for $Hg^0$ (liquid droplets (Ottaviano et al., 1994)), $Hg^{II}$ (HgO), and mercury (added as $Hg^{II}$) in a green rust suspension (bottom).

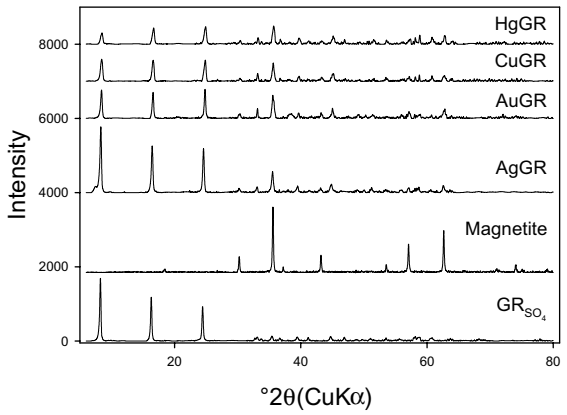


Fig. 2. Comparison of XRD patterns of $GR_{SO_4}$ and magnetite with the patterns of AgGR, AuGR, CuGR, and HgGR. Scans were made between 6° and 80° at a rate of 1° $min^{-1}$.

AuGR, CuGR, and HgGR samples and $Ag^0$, $Au^0$, $Cu^0$, and $Hg^0$ standards are shown in Fig. 3. The close agreement between the XAFS spectra of the metal standards and the AgGR, AuGR, CuGR, and HgGR samples indicates that the average local environment about Ag, Au, Cu, and Hg atoms in the green rust samples is similar to that in the bulk $Ag^0$, $Au^0$, $Cu^0$, and $Hg^0$ phases. Moreover, the majority of the $Ag^0$, $Au^0$, $Cu^0$, and $Hg^0$ phases formed by the reduction of $Ag^I$, $Au^{III}$, $Cu^{II}$, and $Hg^{II}$ by green rust in these samples have crystalline order greater than 5–10 nm.

The formation of nanometer-sized particles of $Ag^0$, $Au^0$, and $Cu^0$ was observed in TEM images of AgGR, AuGR, and CuGR samples (Figs. 4–6, respectively). The identity of individual particles was confirmed by EDX analysis. Although they were not within the field of view in all of the TEM images shown, particles of magnetite (identified by either morphology or electron diffraction) were observed in all of the samples examined, which is consistent with the results of the XRD analysis of bulk AgGR, AuGR, and CuGR samples (Fig. 2). Typically, the $Ag^0$ particles were multiply twinned and irregular in shape and ranged in size from ~40 to 100 nm along the longest dimension. The $Au^0$ particles were also irregularly shaped but 15–30 nm in length. The multiply twinned $Cu^0$ particles were typically spherical and on the order of 10 nm in diameter. Because of the volatility of $Hg^0$, no attempt was made to image HgGR samples.

## 4. Discussion

Few studies have considered the reduction of $Ag^I$ and $Au^{III}$ by structural $Fe^{II}$; however, the reduction of $Ag^I$ and $Au^{III}$ species by metal sulfide minerals has been studied extensively (Jean and Bancroft, 1985; Hiskey

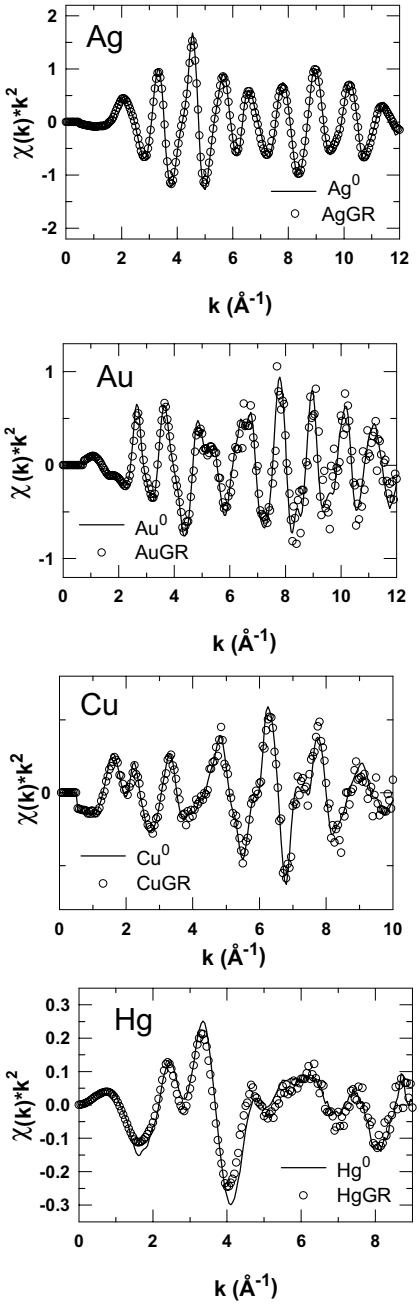


Fig. 3. Average $\chi(k) * k^2$ data for $Ag^0$ and AgGR (top), $Au^0$ and AuGR (second from top), $Cu^0$ and CuGR (second from bottom), and $Hg^0$ and HgGR (bottom).

et al., 1987; Buckley et al., 1989; Bancroft and Hyland, 1990; Mycroft et al., 1995; Scaini et al., 1995, 1997; Maddox et al., 1998). The formation of nano-scale particles of $Au^0$ is commonly observed after the reduction of $Au^{III}$ by pyrite, galena, and arsenopyrite (Mycroft et al., 1995; Scaini et al., 1997; Maddox et al., 1998). Similarly, the reduction of $Ag^I$ by pyrite, galena, and sphalerite typically results in the formation of nano- to micron-scale particles of $Ag^0$ (Hiskey et al., 1987; Buckley et al., 1989; Scaini et al., 1995, 1997). The reduction of $Au^{III}$ and $Ag^I$ by metal sulfide minerals is an important process controlling the concentrations of gold and silver in anoxic aqueous environments and under certain conditions may be responsible for the development of native gold and silver deposits (Bancroft and Hyland, 1990, and references therein). Despite a paucity of studies examining the interaction of $Ag^I$ and $Au^{III}$ species with $Fe^{II}$-bearing minerals (with the exception of $Fe^{II}$ sulfide minerals), the facile reduction of $Ag^I$ and $Au^{III}$ by green rust observed in our experiments suggests that the reduction of $Ag^I$ and $Au^{III}$ to $Ag^0$ and $Au^0$ can also occur in suboxic environments under iron-reducing conditions.

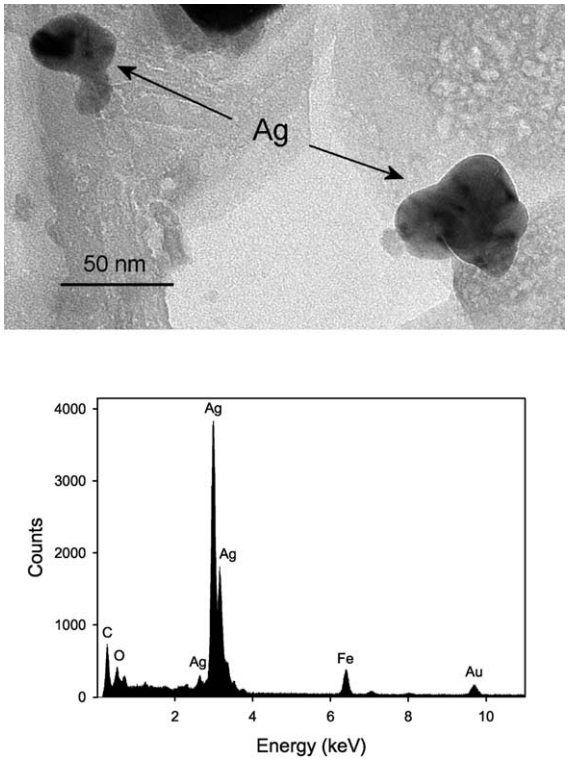


Fig. 4. TEM results for AgGR. Bright-field image showing $Ag^0$ particles (top). EDX spectrum of an Ag particle (bottom); C and Au signals are from the TEM grid, and Fe and O signals are from GR.

Although the reduction of $Ag^I$ and $Au^{III}$ by pyrite yields elemental silver and gold, $Cu^{II}$ is reduced by pyrite only to $Cu^I$ (Voigt et al., 1994; Weisener and Gerson, 2000). However, structural $Fe^{II}$ in phyllosilicates (e.g., biotite and smectite) has been shown to reduce $Cu^{II}$ to elemental copper (Ilton et al., 1992; Markl and Bucher, 1997). Indeed, the reduction of dissolved $Cu^{II}$ to $Cu^0$ by

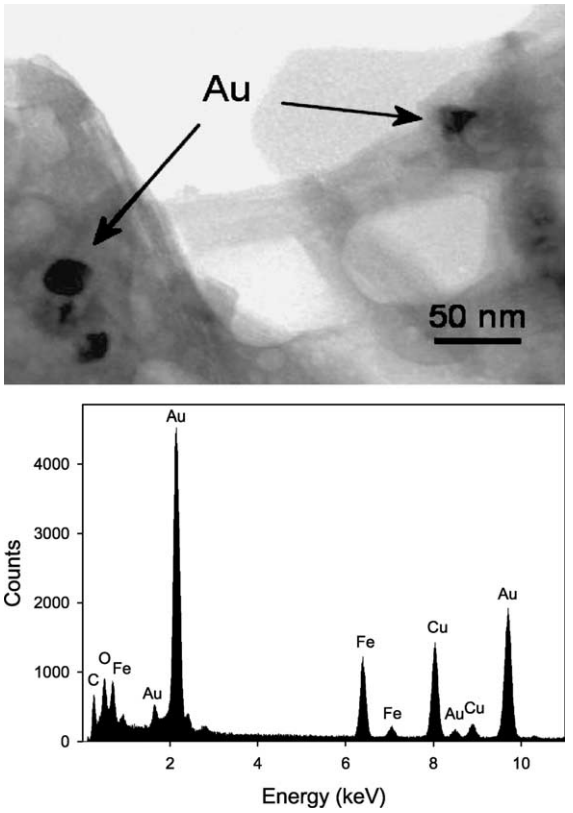


Fig. 5. TEM results for AuGR. Bright-field image showing $Au^0$ particles (top). EDX spectrum of an Au particle (bottom); Cu and C signals are from the TEM grid, and Fe and O signals are from GR.

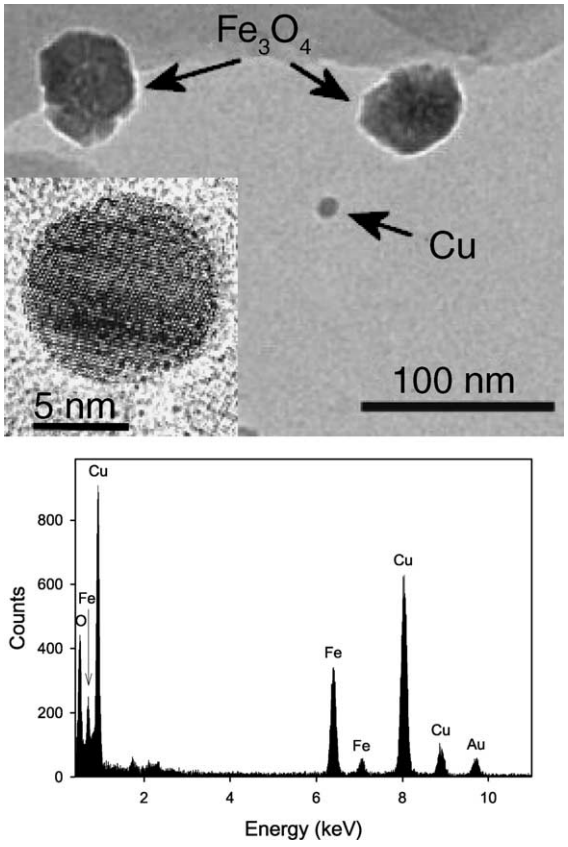


Fig. 6. TEM results for CuGR. Bright-field image showing a $Cu^0$ particle (top) with a high resolution image of the $Cu^0$ particle oriented near (1 1 0) revealing lattice fringe and multiple twinning of the particle (inset). EDX spectrum of a Cu particle (bottom); Au signals are from the TEM grid, and Fe and O signals are from GR.

structural $Fe^{II}$ accompanying the weathering of biotite is believed to be a significant process in the formation of certain porphyry copper deposits (Ilton and Veblen, 1993). The ability of green rust to reduce $Cu^{II}$ and the presence of green rusts in hydromorphic soils and sediments suggests that elemental copper may form from the reduction of $Cu^{II}$ under iron-reducing conditions.

The reduction of $Hg^{II}$ to elemental mercury in aquatic and terrestrial environments results from both abiotic and microbially mediated reactions and is a key component of the biogeochemical cycling of mercury (Stein et al., 1996; Schlüter, 2000). As discussed previously, metal sulfide minerals can reduce $Ag^{I}$ to $Ag^0$, $Au^{III}$ to $Au^0$, and $Cu^{II}$ to $Cu^{I}$, however, although the reduction of $Hg^{II}$ to $Hg^0$ by pyrite is thermodynamically favorable, studies of the interaction of $Hg^{II}$ species with metal sulfide minerals indicate that reduction to $Hg^0$ does not occur (Hyland et al., 1990; Behra et al., 2001). The reduction of $Hg^{II}$ to $Hg^0$ in soils and sediments is generally attributed to direct microbial processes, however, several studies have shown that humic and fulvic acids can abiotically reduce $Hg^{II}$ (Alberts et al., 1974; Skogerboe and Wilson, 1981; Allard and Arsenie, 1991; Rocha et al., 2000). Few studies have examined the reduction of $Hg^{II}$ by environmentally significant $Fe^{II}$ species (Jonasson, 1970), even though the reduction of $Hg^{II}$ to $Hg^0$ by many $Fe^{II}$ species is energetically favorable. We believe that we are the first to show the reduction of $Hg^{II}$ to $Hg^0$ by an environmentally relevant $Fe^{II}$-containing mineral. Furthermore, although additional studies are needed to determine the overall significance of abiotic $Hg^{II}$ reduction by green rusts (and possibly other $Fe^{II}$-bearing minerals, as well as sorbed $Fe^{II}$) in the biogeochemical cycling of mercury, the reduction of $Hg^{II}$ to $Hg^0$ by green rust indicates the potential for abiotic $Hg^{II}$ reduction in $Fe^{II}$-rich suboxic soils and sediments.

The mobility of a chemical species in aquatic and terrestrial environments is dependent on the solution-phase chemistry and the mineralogical composition of a given soil/sediment matrix. Soluble $Ag^{I}$, $Au^{III}$, and $Cu^{II}$

species are often relatively mobile, thus reduction to comparatively insoluble $Ag^0$, $Au^0$, and $Cu^0$ phases can be expected to reduce the mobility of silver, gold, and copper. However, unlike $Ag^0$, $Au^0$, and $Cu^0$, $Hg^0$ is relatively soluble in aqueous solutions. Moreover, $Hg^0$ has a significant vapor pressure and can be lost from aquatic and terrestrial systems through volatilization. Thus, the reduction of $Hg^{II}$ to $Hg^0$ by green rust may actually increase the overall mobility of mercury; indeed, the release of $Hg^0$ vapor to the atmosphere is a significant component of the global cycling of mercury (Stein et al., 1996; Schlüter, 2000).

Clearly, additional research is required to determine the significance of the role of $Fe^{II}$ species such as green rust in the biogeochemical cycling of silver, gold, copper, and mercury. However, the facile reduction of $Ag^I$, $Au^{III}$, $Cu^{II}$, and $Hg^{II}$ by green rusts suggests that the mobility of silver, gold, copper, and mercury can be controlled by $Ag^0$, $Au^0$, $Cu^0$, and $Hg^0$ phases under conditions conducive for the formation of green rusts, namely transitional zones between oxic and anoxic conditions in iron-rich soils and sediments.

## Acknowledgements

The authors thank Maxim Boyanov of the Department of Physics at the University of Notre Dame, as well as Nadia Leyarowska, Holger Tostmann, and Jeff Terry of the MR-CAT at the APS for their assistance in collecting the XAFS data. We also thank Karen Haugen of Argonne National Laboratory and two anonymous reviewers, whose insight and commentary greatly improved the quality and clarity of this paper. Microstructural characterization was carried out at the Electron Microscopy Collaborative Research Center at Argonne. This work was supported by the DOE Office of Science, Office of Biological and Environmental Research, NABIR Program, under contract W-31-109-Eng-38. Work at the MR-CAT beamline was supported, in part, by funding from DOE under grant number DE-FG02-00-ER45811. Use of the APS was supported by the DOE Office of Science, Office of Basic Energy Sciences, under contract W-31-109-Eng-38.

## References

Abdelmoula, M., Trolard, F., Bourrié, G., Génin, J.-M.R., 1998. Evidence for the Fe(II)–Fe(III) green rust "Fougerite" mineral occurrence in a hydromorphic soil and its transformation with depth. Hyp. Int. 112, 235–238.

Alberts, J.J., Schindler, J.E., Miller, R.W., 1974. Elemental mercury evolution mediated by humic acid. Science 184, 895.

Allard, B., Arsenie, I., 1991. Abiotic reduction of mercury by humic substances in aquatic system—an important process for the mercury cycle. Water, Air, Soil Pollut. 56, 457–464.

Bancroft, G.M., Hyland, M.M., 1990. Spectroscopic studies of adsorption/reduction reactions of aqueous metal complexes on sulfide surfaces. In: Hochella, M.F.J., White, A.F. (Eds.), Mineral–Water Interface Geochemistry. American Mineralogical Society, Washington, DC, pp. 511–558.

Behra, P., Bonnissel-Gissinger, P., Alnot, M., Revel, R., Ehrhardt, J.J., 2001. XPS and XAS study of the sorption of Hg(II) onto pyrite. Langmuir 17, 3970–3979.

Bourrié, G., Trolard, F., Génin, J.-M.R., Jaffrezic, A., Maître, V., Abdelmoula, M., 1999. Iron control by equilibria between hydroxy-green rusts and solutions in hydromorphic soils. Geochim. Cosmochim. Acta 63, 3417–3427.

Buckley, A.N., Wouterlood, H.J., Woods, R., 1989. The interaction of pyrite with solutions containing silver ions. J. Appl. Electrochem. 19, 744–751.

Chaudhuri, S.K., Lack, J.G., Coates, J.D., 2001. Biogenic magnetite formation through anaerobic biooxidation of Fe(II). Appl. Environ. Microbiol. 67, 2844–2848.

Cross, J.L., Frenkel, A.I., 1998. Use of scattered radiation for absolute energy calibration. Rev. Sci. Instrum. 70, 38–40.

Durham, P.J., 1988. Theory of XANES. In: Koningsberger, DC, Prins, R. (Eds.), X-Ray Absorption: Principles, Applications, Techniques of EXAFS, SEXAFS and XANES. John Wiley and Sons, New York, pp. 53–84.

Erbs, M., Hansen, H.C.B., Olsen, C.E., 1999. Reductive dechlorination of carbon tetrachloride using iron(II) iron(III) hydroxide sulfate (green rust). Environ. Sci. Technol. 33, 307–311.

Fredrickson, J.K., Zachara, J.M., Kennedy, D.W., Dong, H., Onstott, T.C., Hinman, N.W., Li, S.-M., 1998. Biogenic iron mineralization accompanying the dissimilatory reduction of hydrous ferric oxide by a groundwater bacterium. Geochim. Cosmochim. Acta 62, 3239–3257.

Glasauer, S., Langley, S., Beveridge, T.J., 2002. Intracellular iron minerals in a dissimilatory iron-redcuing bacterium. Science 295, 117–119.

Hansen, H.C.B., Koch, C.B., 1998. Reduction of nitrate to ammonium by sulphate green rust: activation energy and reaction mechanism. Clay Miner. 33, 87–101.

Hansen, H.C.B., Borggaard, O.K., Sorensen, J., 1994. Evaluation of the free energy of formation of Fe(II)–Fe(III) hydroxide-sulphate (green rust) and its reduction of nitrite. Geochim. Cosmochim. Acta 58, 2599–2608.

Hansen, H.C.B., Guldberg, S., Erbs, M., Bender Koch, C., 2001. Kinetics of nitrate reduction by green rusts—Effects of interlayer anion and Fe(II):Fe(III) ratio. Appl. Clay Sci. 18, 81–91.

Hering, J.G., Stumm, W., 1990. Oxidative and reductive dissolution of minerals. In: Hochella, M.F.J., White, A.F. (Eds.), Mineral–Water Interface Geochemistry. American Mineralogical Society, Washington, DC, pp. 427–465.

Hiskey, J.B., Phule, P.P., Pritzker, M.D., 1987. Studies on the effect of addition of silver ions on the direct oxidation of pyrite. Metall. Trans. 18B, 641–647.

Hyland, M.M., Jean, G.E., Bancroft, G.M., 1990. XPS and AES studies of Hg(II) sorption and desorption reactions on sulphide minerals. Geochim. Cosmochim. Acta 54, 1957–1967.

Ilton, E.S., Veblen, D.R., 1993. Origin and mode of copper enrichment in biotite from rocks associated with porphyry copper deposits: a transmission electron microscopy investigation. Econ. Geol. 88, 886–900.

Ilton, E.S., Earley III, D., Marozas, D., Veblen, D.R., 1992. Reaction of some trioctahedral micas with copper sulfate solutions at 25 °C and 1 atmosphere: an electron microprobe and transmission electron microscopy investigation. Econ. Geol. 87, 1813–1829.

Jean, G.E., Bancroft, G.M., 1985. An XPS and SEM study of gold deposition at low temperatures on sulfide mineral surfaces: concentration of gold by adsorption/reduction. Geochim. Cosmochim. Acta 49, 979–987.

Jonasson, I.R., 1970. Mercury in natural environments: a review of recent work. Geol. Surv. Can., Paper 70-57.

Kukkadapu, R.K., Zachara, J.M., Smith, S.C., Fredrickson, J.K., Liu, C., 2001. Dissimilatory bacterial reduction of Al-substituted goethite in subsurface sediments. Geochim. Cosmochim. Acta 65, 2913–2924.

Loyaux-Lawniczak, S., Refait, P., Lecomte, P., Ehrhardt, J.-J., Génin, J.-M.R., 1999. The reduction of chromate ions by Fe(II) layered hydroxides. Hydrol. Earth Syst. Sci. 3, 593–599.

Loyauz-Lawniczak, S., Refait, P., Ehrhardt, J.-J., Lecomte, P., Génin, J.-M.R., 2000. Trapping of Cr by formation of ferrihydrite during the reduction of chromate ions by Fe(II)–Fe(III) hydroxysalt green rusts. Environ. Sci. Technol. 34, 438–443.

Lyngkilde, J., Christensen, T.H., 1992. Redox zones of a landfill leachate pollution plume (Vejen, Denmark). J. Contam. Hydrol. 10, 273–289.

Maddox, L.M., Bancroft, G.M., Scaini, M.J., Lorimer, J.W., 1998. Invisible gold: comparison of Au deposition on pyrite and arsenopyrite. Am. Mineral. 83, 1240–1245.

Markl, G., Bucher, K., 1997. Reduction of $Cu^{2+}$ in mine waters by hydrolysis of ferrous sheet silicates. Eur. J. Mineral. 9, 1227–1235.

Mycroft, J.R., Bancroft, G.M., McIntyre, N.S., Lorimer, J.W., 1995. Spontaneous deposition of gold on pyrite from solutions containing Au(III) and Au(I) chlorides: Part I: A surface study. Geochim. Cosmochim. Acta 59, 3351–3365.

Myneni, S.C.B., Tokunaga, T.K., Brown Jr., G.E., 1997. Abiotic selenium redox transformations in the presence of Fe(II,III) oxides. Science 278, 1106–1109.

Newville, M., 2001. IFEFFIT: Interactive XAFS analysis and FEFF fitting. J. Synchrotron Rad. 8, 322–324.

Newville, M., Livinš, P., Yacoby, Y., Rehr, J.J., Stern, E.A., 1993. Near-edge X-ray absorption fine structure of Pb: a comparison of theory and experiment. Phys. Rev. B 47, 14126–14131.

O'Loughlin, E.J., Burris, D.R., in press. Reduction of halogenated ethanes by green rust. Environ. Toxicol. Chem.

O'Loughlin, E.J., Kemner, K.M., Burris, D.R., 2003. Effects of $Ag^{I}$, $Au^{III}$, and $Cu^{II}$ on the reductive dechlorination of carbon tetrachloride by green rust. Environ. Sci. Technol. 37, 2905–2912.

O'Loughlin, E.J., Kelly, S.D., Csencsits, R., Cook, R.E., Kemner, K.M., 2003. Reduction of uranium(VI) by mixed iron(II)/iron(III) hydroxide (green rust): Formation of $UO_2$ nanoparticles. Environ. Sci. Technol. 37, 721–727.

Ona-Nguema, G., Abdelmoula, M., Jorand, F., Benali, O., Géhin, A., Block, J.-C., Génin, J.-M.R., 2002. Iron(II,III) hydroxycarbonate green rust formation and stabilization from lepidocrocite bioreduction. Environ. Sci. Technol. 36, 16–20.

Ottaviano, L., Filipponi, A., Di Cicco, A., 1994. Supercooling of liquid-metal droplets for X-ray-absorption-spectroscopy investigations. Phys. Rev. B 49, 11749–11758.

Parmar, N., Gorby, Y.A., Beveridge, T.J., Ferris, F.G., 2001. Formation of green rust and immobilization of nickel in response to bacterial reduction of hydrous ferric oxide. Geomicrobiol. J. 18, 375–385.

Peterson, M.L., Brown Jr, G.E., Parks, G.A., 1996. Direct XAFS evidence for heterogeneous redox reaction at the aqueous chromium/magnetite interface. Colloid. Surf. A: Physiochem. Eng. Aspects 107, 77–88.

Ponnamperuma, F.N., Tianco, E.M., Loy, T., 1967. Redox equilibria in flooded soils: 1. The iron hydroxide systems. Soil Sci. 103, 374–382.

Refait, P., Simon, L., Génin, J.-M.R., 2000. Reduction of $SeO_4^{2-}$ anions and anoxic formation of iron(II)–iron(III) hydroxy-selenate green rust. Environ. Sci. Technol. 34, 819–825.

Rocha, J.C., Junior, É.S., Zara, L.F., Rosa, A.H., dos Santos, A., Burba, P., 2000. Reduction of mercury(II) by tropical river humic substances (Rio Nego)—a possible process of the mercury cycle in Brazil. Talanta 53, 551–559.

Rügge, K., Hofstetter, T.B., Haderlein, S.B., Bjerg, P.L., Knudsen, S., Zraunig, C., Mosbæk, H., Christensen, T.H., 1998. Characterization of predominant reductants in an anaerobic leachate-contaminated aquifer by nitroaromatic probe compounds. Environ. Sci. Technol. 32, 23–31.

Scaini, M.J., Bancroft, G.M., Lorimer, J.W., Maddox, L.M., 1995. The interaction of aqueous silver species with sulphur-containing minerals as studied by XPS, AES, SEM, and electrochemistry. Geochim. Cosmochim. Acta 59, 2733–2747.

Scaini, M.J., Bancroft, G.M., Knipe, S.W., 1997. An XPS, AES, and SEM study of the interactions of gold and silver chloride species with PbS and $FeS_2$: Comparison to natural samples. Geochim. Cosmochim. Acta 61, 1223–1231.

Schlüter, K., 2000. Review: evaporation of mercury from soils. An integration and synthesis of current knowledge. Environ. Geol. 39, 249–271.

Segre, C.U., Leyarovska, N.E., Chapman, L.D., Lavender, W.M., Plag, P.W., King, A.S., Kropf, A.J., Bunker, B.A., Kemner, K.M., Dutta, P., Duran, R.S., Kaduk, J., 2000. The MRCAT insertion device beamline at the Advanced Photon Source. In: Pianetta, P.A., Arthur, J.R., Brennan, S. (Eds.), Synchrotron Radiation Instrumentation: Eleventh US National Conference. American Institute of Physics, New York, pp. 419–422.

Skogerboe, R.K., Wilson, S.A., 1981. Reduction of ionic species by fulvic acid. Anal. Chem. 53, 228–232.

Stein, E.D., Cohen, Y., Winer, A.M., 1996. Environmental distribution and transformation of mercury compounds. Crit. Rev. Environ. Sci. Technol. 26, 1–43.

Stern, E.A., 1988. Theory of EXAFS. In: Koningsberger, D.C., Prins, R. (Eds.), X-Ray Absorption: Principles, Applications, Techniques of EXAFS, SEXAFS and XANES. John Wiley and Sons, New York, pp. 3–51.

Stern, E.A., Heald, S.M., 1979. X-ray filter assembly for fluorescence measurements of X-ray absorption fine structure. Rev. Sci. Instrum. 50, 1579–1583.

Taylor, R.W., Shen, S., Bleam, W.F., Tu, S.-I., 2000. Chromate removal by dithionate-reduced clays: Evidence from direct X-ray adsorption near edge spectroscopy (XANES) of chromate reduction at clay surfaces. Clays Clay Miner. 48, 648–654.

Trolard, F., Génin, J.-M.R., Abdelmoula, M., Bourrié, G., Humbert, B., Herbillon, A., 1997. Identification of a green rust mineral in a reductomorphic soil by Mössbauer and Raman spectroscopies. Geochim. Cosmochim. Acta 61, 1107–1111.

Voigt, S., Szargan, R., Suoninen, E., 1994. Interaction of copper(II) ions with pyrite and its influence on ethyl xanthate adsorption. Surf. Interface Anal. 21, 526–536.

Weisener, C., Gerson, A., 2000. Cu(II) adsorption mechanism on pyrite: An EXAFS and XPS study. Surf. Interface Anal. 30, 454–458.

White, A.F., Peterson, M.L., 1996. Reduction of aqueous transition metal species on the surfaces of Fe(II)-containing oxides. Geochim. Cosmochim. Acta 60, 3799–3814.

Williams, A.G.B., Scherer, M.M., 2001. Kinetics of Cr(VI) reduction by carbonate green rust. Environ. Sci. Technol.